Missouri University of Science and Technology
Scholars' Mine

Mechanical and Aerospace Engineering Faculty Research & Creative Works

Mechanical and Aerospace Engineering

01 Jan 2006

A Non-Intrusive Polynomial Chaos Method for Uncertainty Propagation in CFD Simulations

Serhat Hosder
Missouri University of Science and Technology, hosders@mst.edu

R. Perez

Robert W. Walters

Follow this and additional works at: https://scholarsmine.mst.edu/mec_aereng_facwork

 Part of the Aerospace Engineering Commons, and the Mechanical Engineering Commons

Recommended Citation

S. Hosder et al., "A Non-Intrusive Polynomial Chaos Method for Uncertainty Propagation in CFD Simulations," *Proceedings of the 44th AIAA Aerospace Sciences Meeting and Exhibit (2006, Reno, NV)*, American Institute of Aeronautics and Astronautics (AIAA), Jan 2006.
The definitive version is available at https://doi.org/10.2514/6.2006-891

This Article - Conference proceedings is brought to you for free and open access by Scholars' Mine. It has been accepted for inclusion in Mechanical and Aerospace Engineering Faculty Research & Creative Works by an authorized administrator of Scholars' Mine. This work is protected by U. S. Copyright Law. Unauthorized use including reproduction for redistribution requires the permission of the copyright holder. For more information, please contact scholarsmine@mst.edu.

44th AIAA Aerospace Sciences Meeting and Exhibit
9 - 12 January 2006, Reno, Nevada

AIAA 2006-891

A Non-Intrusive Polynomial Chaos Method For Uncertainty Propagation in CFD Simulations

Serhat Hosder*, Robert W. Walters† and Rafael Perez‡
Virginia Polytechnic Institute and State University, Blacksburg, VA, 24061, USA

An inexpensive non-intrusive polynomial chaos (NIPC) method for the propagation of input uncertainty in CFD simulations is presented. The method is straightforward to implement for any stochastic fluid dynamics problem and computationally less expensive than sampling or quadrature based non-intrusive methods. To validate the present NIPC approach, the method has been applied to: (1) an inviscid oblique shock wave problem with geometric uncertainty, (2) an inviscid expansion wave problem with geometric uncertainty, and (3) a subsonic, two-dimensional, laminar boundary layer flow over a flat plate with an uncertain free-stream dynamic viscosity. For all test cases, the statistics (mean and the standard deviation) obtained with the NIPC method were in good agreement with the results of the Monte Carlo simulations. A fourth order polynomial chaos expansion was sufficient to approximate the statistics and the shape of the output uncertainty distributions with the desired accuracy. Only in the shock region of the first test case a sixth order polynomial expansion was required to estimate the statistics of pressure within the 95% confidence intervals of the Monte Carlo results, since the shape of the distributions obtained with 3^{rd} order spatially accurate Euler solutions were highly non-Gaussian in this region.

I. Introduction

A deterministic computational fluid dynamics (CFD) simulation gives a single solution for a certain set of input parameters (the geometry, free-stream flow conditions, angle of attack *etc.*). In real life, these parameters are mostly uncertain and the variability associated with them can have substantial impact on the final result. In addition to the parameter uncertainty, CFD error and uncertainties may also come from discretization errors and mathematical modeling of the physics such as the assumptions in partial differential equations, boundary and initial conditions, and the turbulence models. These factors can also significantly alter the solution of a fluid dynamics problem as shown in studies by Hosder et al[1] and Hemsch.[2] Stochastic CFD simulations are needed to asses the uncertainty in the solution, and to achieve a certain level of robustness or reliability in the final aerodynamic design. Development of credible stochastic aerodynamic simulation tools require effective and efficient methods to model and propagate the input uncertainties, and sufficient testing on various fluid dynamics problems. In this paper, we address this requirement by the introduction and testing of an inexpensive non-intrusive polynomial chaos method developed for the uncertainty propagation in CFD simulations.

Several methods have been used to model and propagate uncertainty in stochastic computational simulations. Interval analysis, propagation of uncertainty using sensitivity derivatives, Monte Carlo simulations, moment methods and polynomial chaos are among the main approaches implemented in CFD simulations. Detailed description and analysis of each method for selected fluid dynamics problems can be found in Walters and Huyse.[3] In this paper we focus on uncertainty propagation with the polynomial chaos (PC) method, which is based on the spectral representation of the uncertainty. Several researchers have studied and implemented the PC approach for a wide range of problems. Ghanem and Spanos[4] (1990) and Ghanem[5,6] (1999) applied the PC method to several problems of interest to the structures community. Mathelin et al.[7] studied uncertainty propagation for a turbulent, compressible nozzle flow by this technique. Xiu and Karniadakis[8]

*Postdoctoral Associate, Aerospace and Ocean Engineering Department, AIAA Member.
†Professor and Department Head, Aerospace and Ocean Engineering Department, AIAA Associate Fellow.
‡Graduate Student, Aerospace and Ocean Engineering Department, AIAA Student Member.

Copyright © 2006 by Serhat Hosder and Robert W. Walters. Published by the American Institute of Aeronautics and Astronautics, Inc., with permission.

analyzed the flow past a circular cylinder and incompressible channel flow by the PC method and extended the method beyond the original formulation of Wiener[9] to include a variety of basis functions. In 2003, Walters[10] applied the PC method to a two-dimensional steady-state heat conduction problem for representing geometric uncertainty. Following this effort, an implicit compact PC formulation was implemented for the stochastic Euler equations (Perez and Walters,[11] 2005).

The PC method for the propagation of uncertainty in computational simulations involves the substitution of uncertain variables and parameters in the governing equations with the polynomial expansions. In general, an intrusive approach will calculate the unknown polynomial coefficients by projecting the resulting equations onto basis functions (orthogonal polynomials) for different modes. As its name suggests, the intrusive approach requires the modification of the deterministic code and this may be inconvenient for many complex computational problems since the modification of the existing code can be difficult, expensive, and time consuming. To alleviate this inconvenience, non-intrusive methods have been investigated by many researchers. Most of the non-intrusive PC approaches in the literature are based on *sampling* (Debusschere et al.,[12] Reagan et. al.,[13] and Isukapalli[14]) or *quadrature* methods (Debusschere et al.[12] and Mathelin et al.[15]) to determine the projected polynomial coefficients.

In this paper, we present an inexpensive non-intrusive Polynomial chaos (NIPC) method for the propagation of input uncertainty. Our approach is not based on sampling or quadrature methods to evaluate the polynomial coefficients. The present method is straightforward to implement in any stochastic fluid dynamics problem and computationally less expensive than sampling or quadrature based methods. To validate the present NIPC approach, we have applied the method to three basic fluid dynamics problems: (1) inviscid oblique shock wave problem with geometric uncertainty, (2) inviscid expansion wave problem with geometric uncertainty, and (3) steady, subsonic, 2-D, zero-pressure gradient laminar boundary layer flow over a flat plate, which has the free-stream dynamic viscosity as the uncertain parameter. In this paper, we first give a brief review of the Hermite Polynomial Chaos and then describe the present method. Following the description, we give the results of the stochastic test problems and end the paper with the conclusions drawn from these cases.

II. Basics of Hermite Polynomial Chaos

Spectral representation of uncertainty in engineering simulations has been studied by many researchers in recent years (See Ghanem,[5,6] Ghanem and Spanos,[4,16] and Xiu and Karniadakis[8,17]). An important aspect of spectral representation of uncertainty is that one may decompose a random function (or variable) into separable deterministic and stochastic components. For example, for any stochastic variable (*i.e.*,α^*) such as velocity, density or pressure with random fluctuations, we can write,

$$\alpha^*(x,y,\vec{\xi}) = \sum_{i=0}^{P} \alpha_i(x,y)\Psi_i(\vec{\xi}) \tag{1}$$

where $\alpha_i(x,y)$ is the deterministic component and$\Psi_i(\vec{\xi})$ is the random basis function corresponding to the i^{th} mode. Here we assume α^* to be a function of deterministic independent variables x and y, and the n-dimensional random variable vector $\vec{\xi} = (\xi_1, ..., \xi_n)$ which has a specific probability distribution. Effectively, in Equation 1, $\alpha_i(x,y)$ is the amplitude of the i^{th} fluctuation. The discrete sum is taken over the number of output modes , $P+1 = \frac{(n+p)!}{n!p!}$, which is a function of the order of polynomial chaos (p) and the number of random dimensions (n). For the basis function, we use multi-dimensional Hermite Polynomial to span the n-dimensional random space, which was first used by Wiener[9,18] in his original work of polynomial chaos. Many other choices are possible for basis functions depending on the type of the probability distribution selected for the input uncertainty (See Xiu and Karniadakis[8] for a detailed description and usage of different basis functions). A convenient form of the Hermite polynomials is given by

$$H_k(\xi_{i_1}, ..., \xi_{i_k}) = e^{\frac{1}{2}\vec{\xi}^T\vec{\xi}}(-1)^k \frac{\delta^k}{\delta\xi_{i_1}...\delta\xi_{i_k}}\left(e^{-\frac{1}{2}\vec{\xi}^T\vec{\xi}}\right) \tag{2}$$

where $k = 0, 1, ..., p$. Table 1 gives Hermite Polynomials of a one-dimensional random variable ξ up to 10 orders.

Table 1. Hermite Polynomials of single variable ξ up to 10 orders.

k	$H_k(\xi)$
0	1
1	ξ
2	$-1+\xi^2$
3	$-3\xi+\xi^3$
4	$3-6\xi^2+\xi^4$
5	$15\xi-10\xi^3+\xi^5$
6	$-15+45\xi^2-15\xi^4+\xi^6$
7	$-105\xi+105\xi^3-21\xi^5+\xi^7$
8	$105-420\xi^2+210\xi^4-28\xi^6+\xi^8$
9	$945\xi-1260\xi^3+378\xi^5-36\xi^7+\xi^9$
10	$-945+4725\xi^2-3150\xi^4+630\xi^6-45\xi^8+\xi^{10}$

The inner product of two functions $f(\vec{\xi})$ and $g(\vec{\xi})$ is defined by

$$\left\langle f(\vec{\xi})g(\vec{\xi})\right\rangle = \int_{-\infty}^{\infty} f(\vec{\xi})g(\vec{\xi})p_N(\vec{\xi})d\vec{\xi} \tag{3}$$

where the weight function $p_N(\vec{\xi})$ is an n-dimensional Gaussian distribution with unit variance:

$$p_N(\vec{\xi}) = \frac{1}{\sqrt{(2\pi)^n}} e^{\frac{1}{2}\vec{\xi}^T\vec{\xi}}. \tag{4}$$

The Hermite polynomials form a complete orthogonal set of basis functions in the random space, therefore the inner product of the basis functions is zero with respect to each other, *i.e.*

$$\langle \Psi_i \Psi_j \rangle = \left\langle \Psi_i^2 \right\rangle \delta_{ij} \tag{5}$$

where δ_{ij} is the Kronecker delta function.

The statistics of the distribution for a flow variable at a spatial location can be calculated after the polynomial coefficients $\alpha_k(x,y)$, $(k=0,1,..,P)$ in Equation 1 are determined. The mean of the random solution is given by

$$\bar{\alpha}^*(x,y) = E_{PC}\left[\alpha^*(x,y,\vec{\xi})\right] = \int_{-\infty}^{\infty} \alpha^*(x,y,\vec{\xi})p_N(\vec{\xi})d\vec{\xi} = \alpha_0(x,y) \tag{6}$$

which indicates that the zeroth mode of the expansion corresponds to the expected value or the mean of $\alpha^*(x,y,\vec{\xi})$. Similarly, the variance of the distribution can be obtained as:

$$Var_{PC}\left[\alpha^*(x,y,\vec{\xi})\right] = \int_{-\infty}^{\infty} \left(\alpha^*(x,y,\vec{\xi}) - \bar{\alpha}^*(x,y)\right)^2 p_N(\vec{\xi})d\vec{\xi} = \sum_{i=1}^{P} \left[\alpha_i^2(x,y) < \Psi_i^2 >\right]. \tag{7}$$

In Equation 6, we have used the fact that $\langle \Psi_k \rangle = 0$ for $k > 0$. Moreover, it can also be shown that $k = 1, 2, ..., n$ modes are the Gaussian estimates of the variance and all higher modes provide non-Gaussian interactions.

To model the uncertainty propagation in CFD or other computational simulations via polynomial chaos with the intrusive approach, all dependent variables and random parameters (such as viscosity, coefficient of heat conduction *etc.*) in the governing equations are replaced with their polynomial chaos expansions. Taking the inner product of the equations, $< \cdot, \Psi_k >$ (or projecting each equation onto k^{th} basis) yield

$P+1$ times the number of deterministic equations which can be solved by the same numerical methods applied to the original deterministic system. Although straightforward in theory, an intrusive formulation for complex problems such as the full Navier-Stokes simulation of 3-D, viscous, turbulent flows around realistic aerospace vehicles, chemically reacting flows, or multi-system level simulations which include the interaction of many different codes from different disciplines can be relatively difficult, expensive, and time consuming to implement. To overcome such inconveniences associated with the intrusive approach, some non-intrusive polynomial chaos formulations have been developed for uncertainty propagation.

The main objective of the non-intrusive polynomial chaos methods is to obtain approximations of the polynomial coefficients without making any modifications to the deterministic code. Two commonly used approaches for non-intrusive polynomial chaos are sampling based and quadrature methods. To find the polynomial coefficients $\alpha_k = \alpha_k(x,y)$, $(k = 0, 1, .., P)$ in Equation 1 using these methods, the equation is projected onto k^{th} basis:

$$\left\langle \alpha^*(x,y,\vec{\xi}), \Psi_k(\vec{\xi}) \right\rangle = \left\langle \sum_{i=0}^{P} \alpha_i \Psi_i(\vec{\xi}), \Psi_k(\vec{\xi}) \right\rangle \tag{8}$$

By the virtue of orthogonality,

$$\left\langle \alpha^*(x,y,\vec{\xi}), \Psi_k(\vec{\xi}) \right\rangle = \alpha_k \left\langle \Psi_k^2(\vec{\xi}) \right\rangle \tag{9}$$

which leads to

$$\alpha_k = \frac{\left\langle \alpha^*(x,y,\vec{\xi}), \Psi_k(\vec{\xi}) \right\rangle}{\left\langle \Psi_k^2(\vec{\xi}) \right\rangle} \tag{10}$$

In sampling based methods, the main strategy is to compute $\alpha^*(x,y,\vec{\xi})\Psi_k(\vec{\xi})$ for a number of samples ($\vec{\xi_i}$ values) and perform averaging to determine the estimate of the inner product $\left\langle \alpha^*(x,y,\vec{\xi}), \Psi_k(\vec{\xi}) \right\rangle$. Quadrature methods calculate the same term, which is an integral over the support of the weight function $P_N(\vec{\xi})$, using Gauss-Hermite Quadrature points. Once this term is evaluated, both methods (sampling based and quadrature) use Equation 10 to estimate the projected polynomial coefficients for each mode.

III. Description of the Present Non-Intrusive Polynomial Chaos Method

The present non-intrusive PC was first introduced by Walters[10] to approximate the polynomial chaos coefficients of the metric terms which are required as input stochastic variables for the intrusive polynomial chaos representation of a stochastic heat transfer problem with geometric uncertainty. In 2005, Walters[19] used the same approach to determine the optimum lift-to-drag ratio for a cosine-shaped airfoil as a function of angle of attack using shock-expansion solutions to demonstrate the optimization and reconstruction via PC. In this paper, we present the method for the propagation of input uncertainty in CFD simulations.

The present NIPC method starts with replacing the uncertain variables of interest with their polynomial expansions given by Equation 1. Then, for a given PC of order P, we choose P+1 vectors $\vec{\xi_i} = \{\xi_1, \xi_2, ..., \xi_n\}_i$, $(i = 0, 1, 2, ..., P)$ in random space and evaluate the deterministic code at these points. With the left hand side of Equation (1) known from the solutions of deterministic evaluations at the chosen random points, a linear system of equations can be obtained:

$$\begin{pmatrix} \Psi_0(\vec{\xi_0}) & \Psi_1(\vec{\xi_0}) & \cdots & \Psi_p(\vec{\xi_0}) \\ \Psi_0(\vec{\xi_1}) & \Psi_1(\vec{\xi_1}) & \cdots & \Psi_p(\vec{\xi_1}) \\ \vdots & \vdots & \ddots & \vdots \\ \Psi_0(\vec{\xi_p}) & \Psi_1(\vec{\xi_p}) & \cdots & \Psi_p(\vec{\xi_p}) \end{pmatrix} \begin{pmatrix} \alpha_0 \\ \alpha_1 \\ \vdots \\ \alpha_p \end{pmatrix} = \begin{pmatrix} \alpha^*(\vec{\xi_0}) \\ \alpha^*(\vec{\xi_1}) \\ \vdots \\ \alpha^*(\vec{\xi_p}) \end{pmatrix} \tag{11}$$

The spectral modes (α_k) of the random variable, α^*, are obtained by solving the linear system of equations given above.

The method described here is non-intrusive in the sense that no modification to the deterministic code is required in any form. In this method, the deterministic code is treated as a *black box*. The new non-intrusive method is straightforward to implement, requires a single LU decomposition on a relatively small matrix,

minimally requires $P+1$ deterministic evaluations to estimate statistics, and can be shown to converge to the *projected* PC expansion coefficients under certain conditions. However, in general, the solution obtained by this non-intrusive approach is not unique, since one can choose the random vectors arbitrarily to evaluate the required deterministic solutions. Because of this fact, the present non-intrusive method should be interpreted as a *model* for estimating the projected coefficients.

IV. Results

To test the performance of this NIPC approach in CFD simulations, we have chosen three basic flow problems. These cases represent three building blocks of fluid dynamics. The first problem is inviscid, steady, supersonic, two-dimensional flow over a wedge which has an uncertainty in the wedge angle and represents a stochastic oblique shock wave problem. The second test case is inviscid, steady, supersonic, two-dimensional flow over an expansion corner with an uncertainty in the corner angle and represents a stochastic expansion wave problem. The last problem is steady, subsonic, two-dimensional, zero-pressure gradient laminar boundary layer flow over a flat plate, which has the free-stream dynamic viscosity as the uncertain parameter.

In all test cases we have compared the polynomial chaos results to the statistics obtained with crude (basic) Monte Carlo simulations. In this approach we have followed the procedure described in Walters and Huyse:[3] (1) sample input random variable from its assumed probability density function, (2) compute deterministic output for each sampled input value, and (3) determine statistics of the output distribution such as the mean and the variance. The Monte Carlo method is known to converge to the exact stochastic solution as the number of samples, $n_s \to \infty$. However, the convergence of the mean error estimate is relatively slow since the standard deviation of the mean scales with the square root of the number of samples,

$$\sigma_u = \frac{\sigma}{\sqrt{n_s}}. \tag{12}$$

We could afford to perform 10,000 Monte Carlo simulations for each problem in order to increase the accuracy in our estimation of the statistics. These Monte Carlo simulations enabled us to test the accuracy of our non-intrusive polynomial chaos approach for the selected problems. However, performing a large number of Monte Carlo simulations would be beyond the reach of current computational power, even with high performance computers, for many realistic aerodynamic problems that require the solution of complex flow fields. This fact is one of the motivations for the development of the polynomial chaos methods to model uncertainty propagation in CFD simulations.

A. Oblique Shock Wave Problem

To analyze the stochastic oblique shock wave problem, we address inviscid, steady, two-dimensional, supersonic flow of a calorically perfect gas over a wedge as shown in Figure 1(a). The deterministic problem includes the solution of the supersonic flow field for a given free stream Mach number (M_{ref}), specific heat ratio (γ), and the wedge angle, θ. The output quantity of interest for this problem is the scaled static pressure distribution in the flow field, P/P_{ref}, where P_{ref} is the free-stream pressure.

1. *Deterministic Problem*

To solve the deterministic problem, one may use the analytical oblique shock relations for a perfect gas, which gives the pressure rise across the shock as a function of M_{ref}, γ, and θ. In our study, we solved the deterministic problem numerically using the CFL3D code of NASA Langley Research Center to demonstrate the application of the present NIPC method to CFD simulations. CFL3D is a three-dimensional, finite-volume Navier-Stokes code capable of solving steady or time-dependent aerodynamic flows ranging from subsonic to supersonic speeds.[20]

We used CFL3D to solve the Euler equations which are a subset of Navier-Stokes equations and govern the inviscid, compressible flow of a fluid. Both NIPC and Monte Carlo methods used the deterministic solutions from Euler calculations in their implementation. The computations were performed on grids which have 65 grid points in both x- and z-directions. Figure 1(b) shows the grid with the mean wedge angle, θ_{mean}. The equations were integrated in time using an implicit approximate factorization scheme to reach the steady state. A full multigrid (multigrid+mesh sequencing) method was used for convergence acceleration.

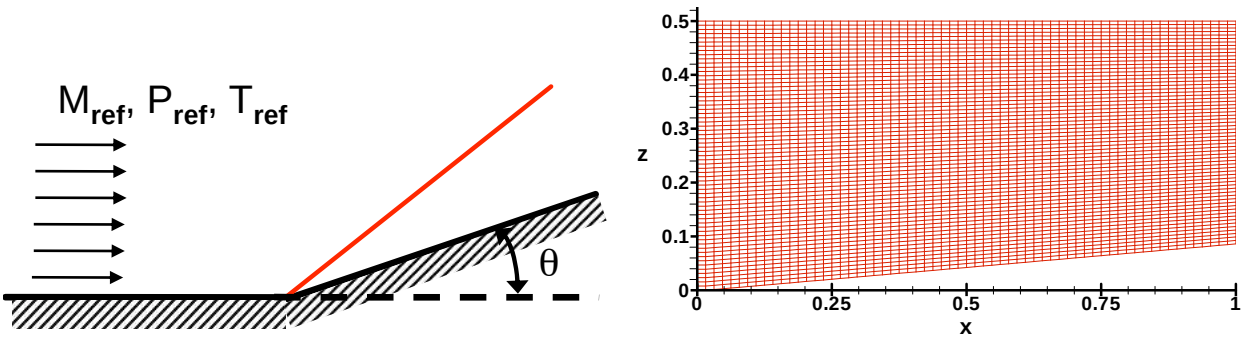

(a) Sketch of supersonic flow and the oblique shock.

(b) The mean grid (65×65) used in Euler computations. The mean wedge angle (θ_{mean}) is 5.0^o.

Figure 1. Description of the supersonic, inviscid flow over a ramp with wedge angle θ.

The inviscid fluxes on the cell-faces were calculated using Roe flux difference splitting.[21] To investigate the effect of spatial accuracy on the stochastic problem, we calculated the primitive variable values on the cell faces using two interpolation schemes: (1) fully upwind 1^{st} order accurate and (2) upwind-biased 3^{rd} order accurate with the $MinMod$ limiter. The MinMod limiter was used for the higher order scheme to eliminate the non-physical oscillations in the shock region. It should be noted that the 3^{rd} order is the nominal order of the scheme but the observed order of accuracy would be more likely to be less than this value due to the multi-dimensionality of the problem, shock wave (discontinuity), and the use of the limiter (See the studies by Hosder[1] and Roy[22] for more on this topic). However, we will still use the nominal orders in the text for the purpose of labelling the cases. The boundary conditions for this problem were set as follows: all flow variables were kept fixed at their free-stream values at the in-flow boundary. The free-steam Mach number was chosen as $M_{ref} = 3.0$ and the angle of attack was set to zero degrees. For the far-field (top) and out-flow surfaces, all flow variables were determined by first-order extrapolation from the interior cells. A wall-tangency boundary condition was prescribed along the bottom surface.

2. Stochastic Problem

The stochastic oblique shock wave problem was formulated by introducing a geometric uncertainty through the wedge angle (θ) that was uncertain and described by a Gaussian distribution:

$$\theta(\xi) = \theta_{mean} + \xi\sigma. \tag{13}$$

The mean wedge angle was 5° and the coefficient of variation was 10%. Here ξ is a normally distributed random variable with zero mean and unit variance ($\xi = N[0, 1]$).

Uncertainty propagation in supersonic wedge flow has been modeled using Monte Carlo and the NIPC methods. In Monte Carlo simulations, 10,000 grids were created using 10,000 samples from the $\theta(\xi)$ distribution. The Euler Equations were solved on each grid using the CFL3D code. It took approximately 55.4 hours (2.3 days) to complete 10,000 Monte Carlo simulations on a Apple© G-5 computer with dual processors. A fourth order polynomial expansion was chosen to model the uncertainty propagation with the NIPC method. To obtain the polynomial coefficients, five deterministic solutions were evaluated on five grids with wedge angles that correspond to $\xi_1 = 0.0$, $\xi_2 = 1.0$, $\xi_3 = -1.0$, $\xi_4 = 2.0$, and $\xi_5 = -2.0$. It took only 2 minutes to complete these runs on the same computer. In addition to the fourth order polynomial chaos evaluation, a parametric study was also performed to see the effect of the order of the polynomial chaos on the statistics of the Euler solutions with 3^{rd} order spatial accuracy.

It should be noted that each deterministic solution that corresponds to a specific value of $\theta(\xi)$ was obtained on a different grid which has different cell center locations. Each deterministic solution was interpolated to the mean grid to calculate the Monte Carlo statistics at the cell center locations of the mean grid. Similarly, the polynomial chaos expansions for the pressure were calculated at the mean grid cell center locations using five deterministic solutions that were obtained from the interpolation of the original $\theta(\xi_i)$ $(i = 1, .., 5)$ results to the mean grid.

The mean pressure contours of the NIPC method and the Monte Carlo simulations are shown in Figure 2. Qualitatively, we see a good agreement between the results of the two methods when the polynomial chaos

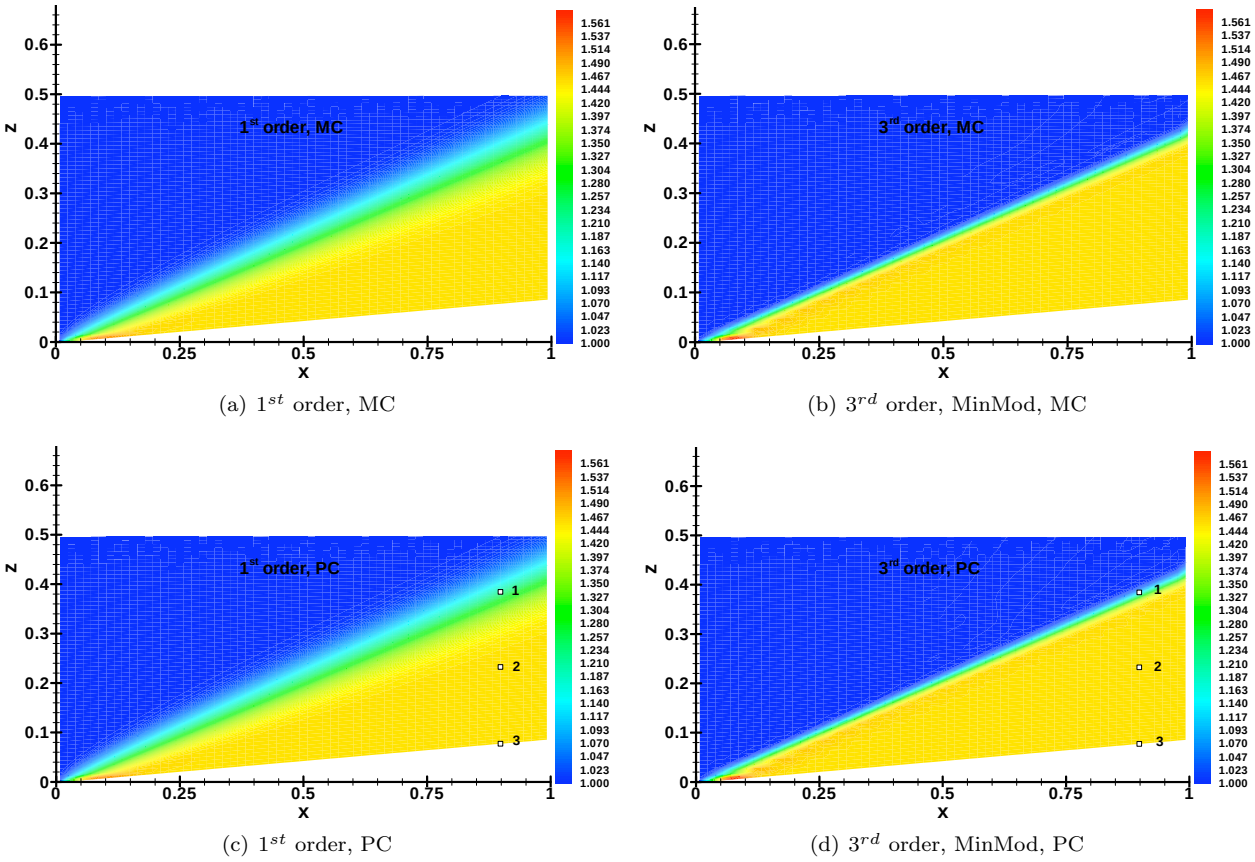

(a) 1^{st} order, MC

(b) 3^{rd} order, MinMod, MC

(c) 1^{st} order, PC

(d) 3^{rd} order, MinMod, PC

Figure 2. Mean pressure (P/P_{ref}) distributions obtained from MC simulations and NIPC expansions for the supersonic ramp problem. Polynomial chaos results are obtained with a 4^{th} order expansion. The three locations showed in the PC plots designate the points where the quantitative analysis were performed.

Table 2. The mean static pressure (P/P_{ref}) values obtained with NIPC and Monte Carlo methods at three selected locations for the supersonic ramp problem. The 95% confidence intervals for the mean values are calculated for Monte Carlo simulations using the Bootstrap method.

Spatial Accuracy	Location	Mean PC	Mean MC	95% Conf. Interval
1^{st} *order*	1	1.21820	1.21821	[1.21714, 1.21934]
	2	1.45411	1.45411	[1.45308, 1.45517]
	3	1.45438	1.45438	[1.45335, 1.45543]
3^{rd} *order with MinMod*	1	1.11433	1.11739	[1.11469, 1.12003]
	2	1.45484	1.45475	[1.45372, 1.45581]
	3	1.45472	1.45471	[1.45368, 1.45577]

and the Monte Carlo solutions are compared for the same spatial accuracy. The mean pressure field obtained with the 1^{st} order spatially accurate Euler solutions show that the static pressure increases smoothly in a relatively wider region. As expected, the 3^{rd} order scheme captures the shock more accurately and the pressure jump occurs in a much smaller region. The contours of standard deviation again show a good qualitative agreement between the Monte Carlo and the polynomial chaos results (Figure 3). The maximum value of the standard deviation obtained from the 3^{rd} order spatially accurate solutions is approximately 2.5 times larger than that of the 1^{st} order results. For the higher order case, the large values of the standard deviation are located in the shock region, especially towards the outflow boundary.

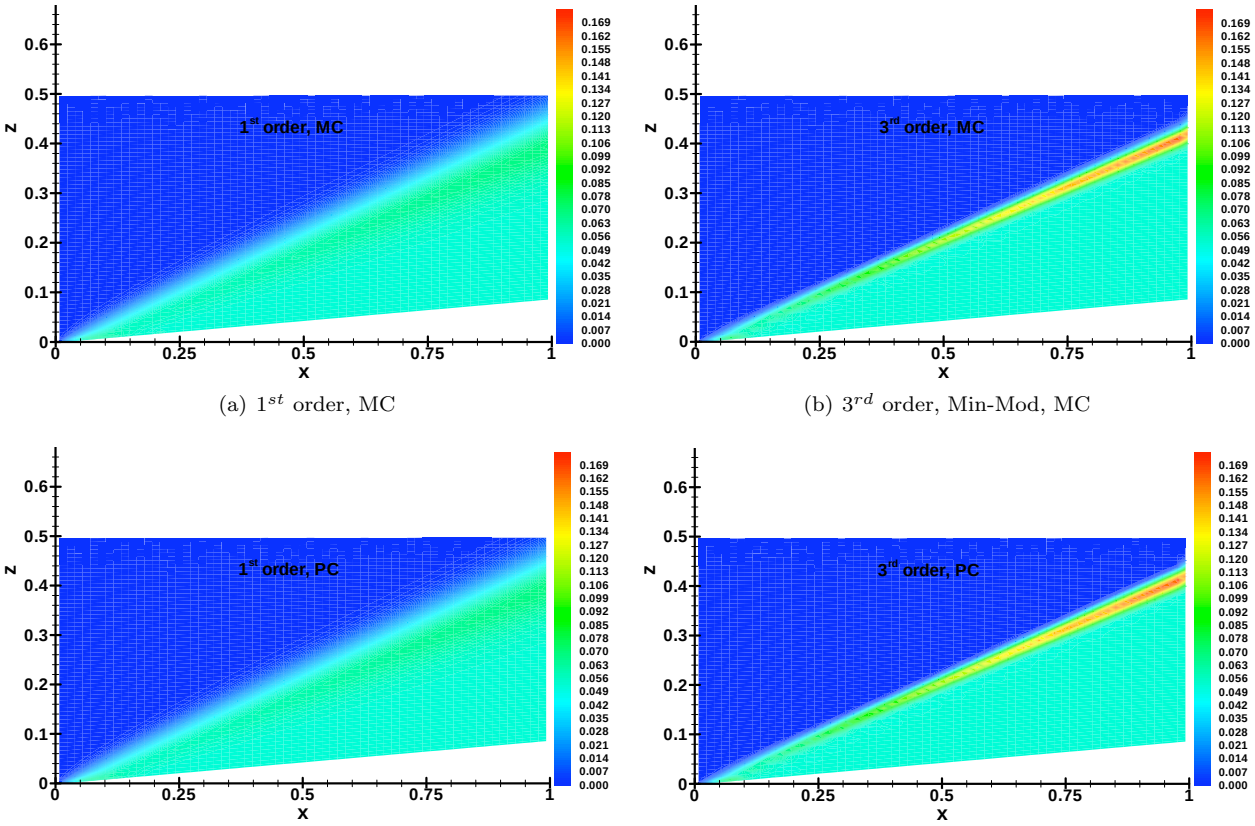

(a) 1^{st} order, MC

(b) 3^{rd} order, Min-Mod, MC

(c) 1^{st} order, PC

(d) 3^{rd} order, Min-Mod, PC

Figure 3. Standard deviation distributions of pressure (P/P_{ref}) obtained from MC simulations and NIPC expansions for the supersonic ramp problem. Polynomial chaos results are obtained with a 4^{th} order expansion.

Table 3. The standard deviation of static pressure (P/P_{ref}) obtained with NIPC and Monte Carlo methods at three selected locations for the supersonic ramp problem. The 95% confidence intervals for the standard deviations are calculated for Monte Carlo simulations using the Bootstrap method.

Spatial Accuracy	Location	StD PC	StD MC	95% Conf. Interval
1^{st} *order*	1	0.0570991	0.057091	[0.0561843, 0.0579676]
	2	0.0524008	0.0523996	[0.051638, 0.0530961]
	3	0.0522568	0.0522547	[0.0514975, 0.0529443]
3^{rd} *order with MinMod*	1	0.140332	0.137809	[0.135184, 0.140262]
	2	0.052422	0.0523684	[0.0516112, 0.0530614]
	3	0.0522727	0.0523118	[0.0515483, 0.0530093]

To analyze the statistics of the Monte Carlo and NIPC methods quantitatively, we have picked three locations in the flow field. All three are on the same streamwise station, but they are at different distances from the wall (Figure 2). Location 1 ($x = 0.8984$, $z = 0.3844$) is in the shock region, Location 2 ($x = 0.8984$, $z = 0.2325$) is downstream of the shock, and Location 3 ($x = 0.8984$, $z = 0.0772$) is a point on the wall downstream of the shock. Figure 4 shows the static pressure histograms at these locations obtained with Monte Carlo and the NIPC methods that use 1^{st} order spatially accurate deterministic Euler solutions. At all locations, the histograms of the polynomial chaos method are essentially the same as the ones obtained with the Monte Carlo simulations. The distribution at location 1 (shock region) is slightly skewed to the right, whereas the histograms at locations 2 and 3 follow the Gaussian distribution closely. The mean and

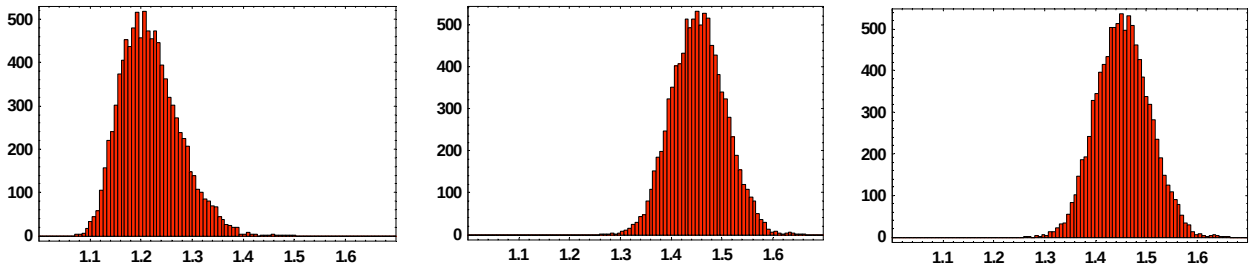

(a) Location 1, MC (b) Location 2, MC (c) Location 3, MC

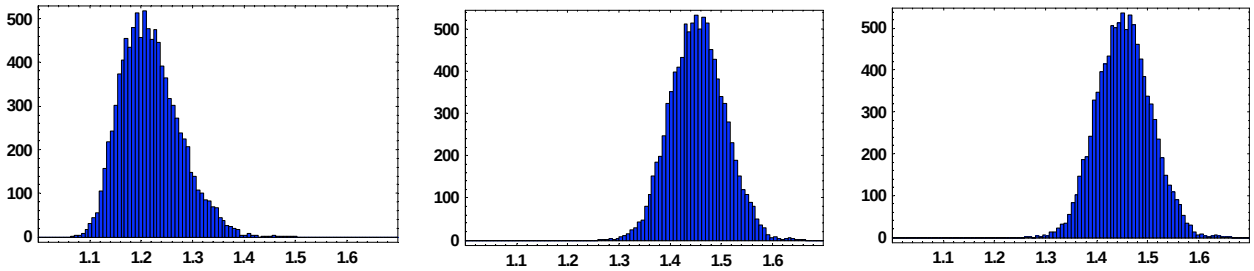

(d) Location 1, PC (e) Location 2, PC (f) Location 3, PC

Figure 4. Static pressure histograms obtained at three locations for the supersonic ramp problem using MC and NIPC methods. The deterministic Euler solutions are calculated using 1^{st} order accurate upwind-biased Roe flux difference splitting. Polynomial chaos results are obtained from a 4^{th} order expansion.

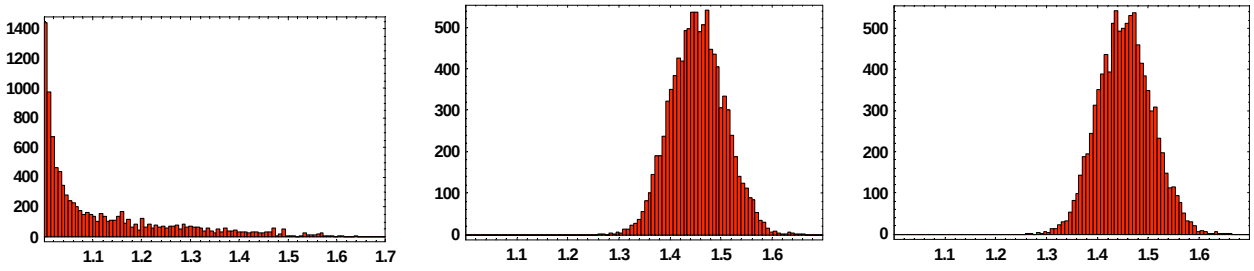

(a) Location 1, MC (b) Location 2, MC (c) Location 3, MC

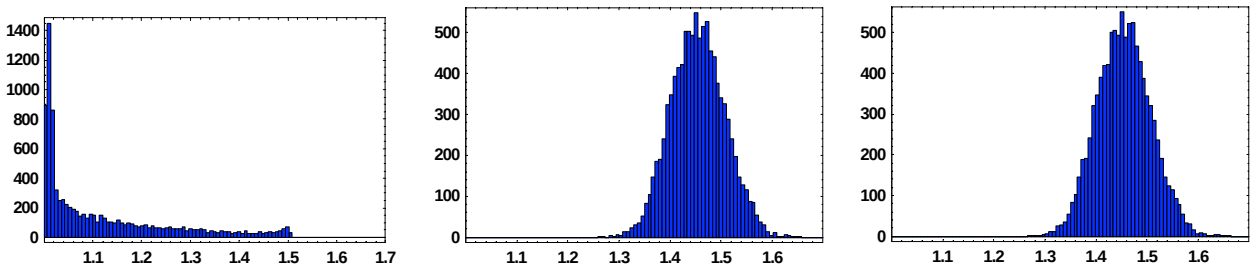

(d) Location 1, PC (e) Location 2, PC (f) Location 3, PC

Figure 5. Static pressure histograms obtained at three locations for the supersonic ramp problem using MC and NIPC methods. The deterministic Euler solutions are calculated using 3^{rd} order accurate upwind-biased Roe flux difference splitting with the MinMod limiter. Polynomial chaos results are obtained from a 4^{th} order expansion.

the standard deviation values of these distributions are given in Tables 2 and 3. For each statistical quantity obtained with the Monte Carlo Simulations, a 95% confidence interval is also presented. We use the *bootstrap method* to compute the confidence intervals as well as the standard error estimate of each statistical quantity. The advantage of this method is that it is not restricted to a specific distribution, e.g. a Gaussian. It is easy and efficient to implement and can be completely automated to any estimator, such as the mean or

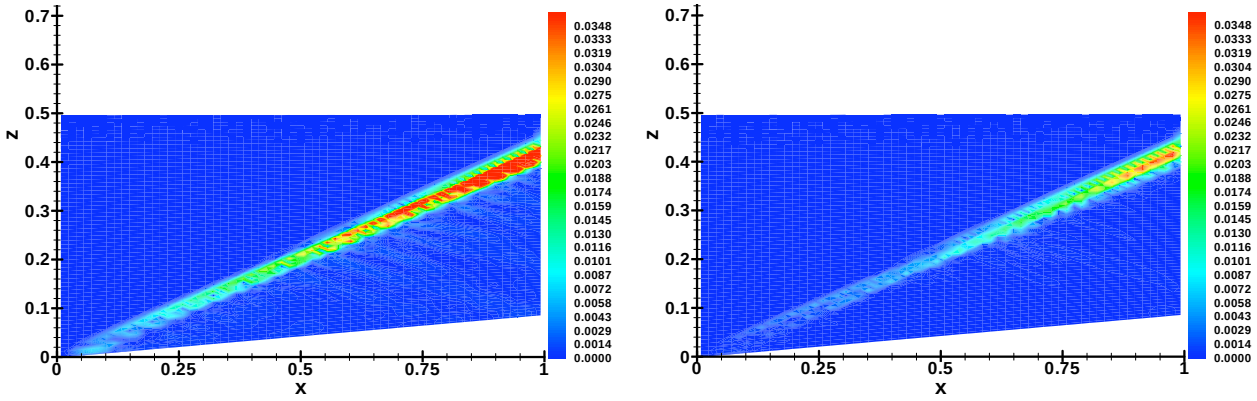

(a) 1^{st} order PC, $\xi = \{0, 1\}$

(b) 2^{nd} order PC, $\xi = \{0, 1, -1\}$

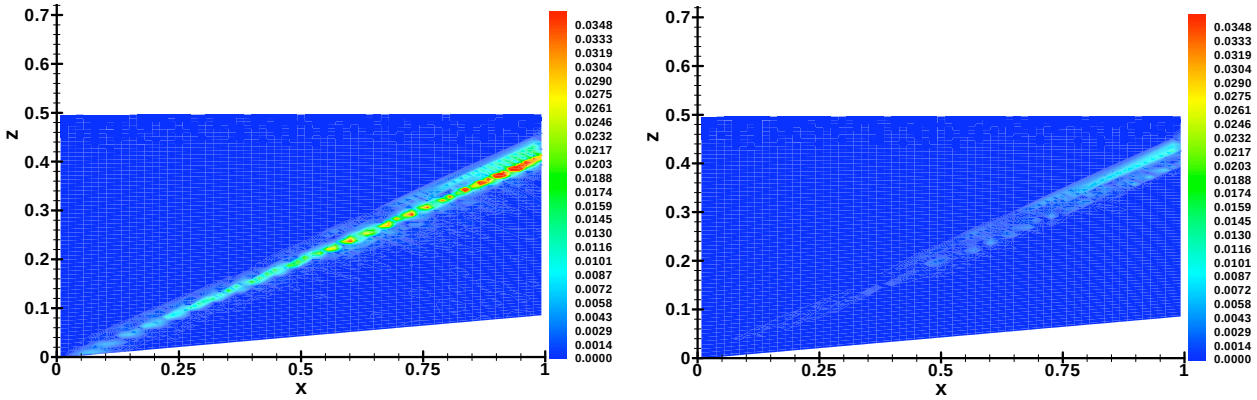

(c) 3^{rd} order PC, $\xi = \{0, 1, -1, 2\}$

(d) 4^{th} order PC, $\xi = \{0, 1, -1, 2, -2\}$

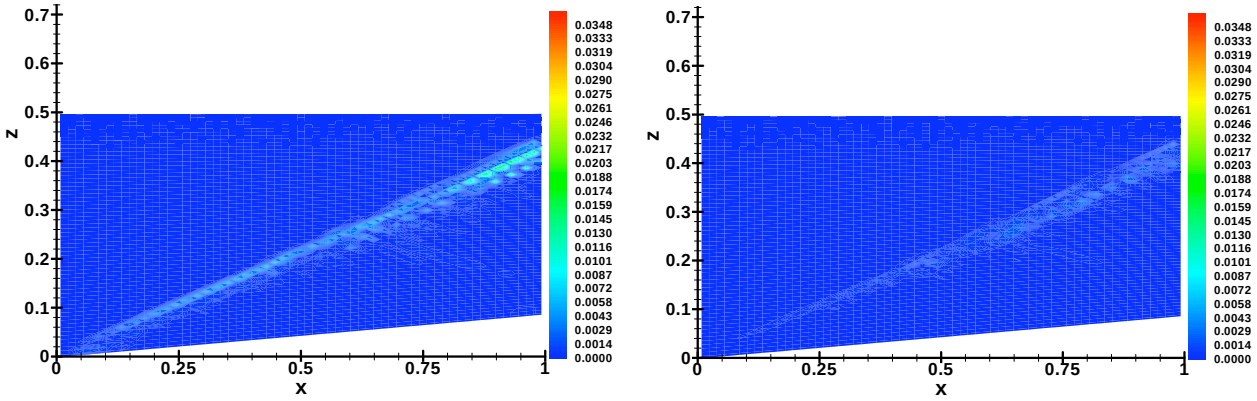

(e) 5^{th} order PC, $\xi = \{0, 1, -1, 2, -2, 3\}$

(f) 6^{th} order PC, $\xi = \{0, 1, -1, 2, -2, 3, -3\}$

Figure 6. The contours showing the difference ($|Std_{MC} - Std_{PC}|$) between the static pressure standard deviation values obtained using MC and NIPC methods for the supersonic ramp problem. The deterministic Euler solutions are calculated using 3^{rd} order accurate upwind-biased Roe flux difference splitting with the MinMod limiter for the selected $\theta\xi$ values.

the variance. In practice, one takes 25–200 bootstrap samples to obtain a standard error estimate. In our computations, we used 500 bootstrap samples. Note that each sample consisted of 10,000 observations selected randomly from the original Monte Carlo simulations by giving equal probability ($1/10,000$) to each observation. All mean and standard deviation values obtained with the NIPC method fall within the 95% confidence interval for 1^{st} order spatially accurate solutions. Figure 5 gives the histograms for the 3^{rd} order accurate Euler solutions. At location 1 where there is large pressure gradient due to the shock (Figure 2), the histograms are highly non-Gaussian and one sided. They are skewed to the right with a large tail region.

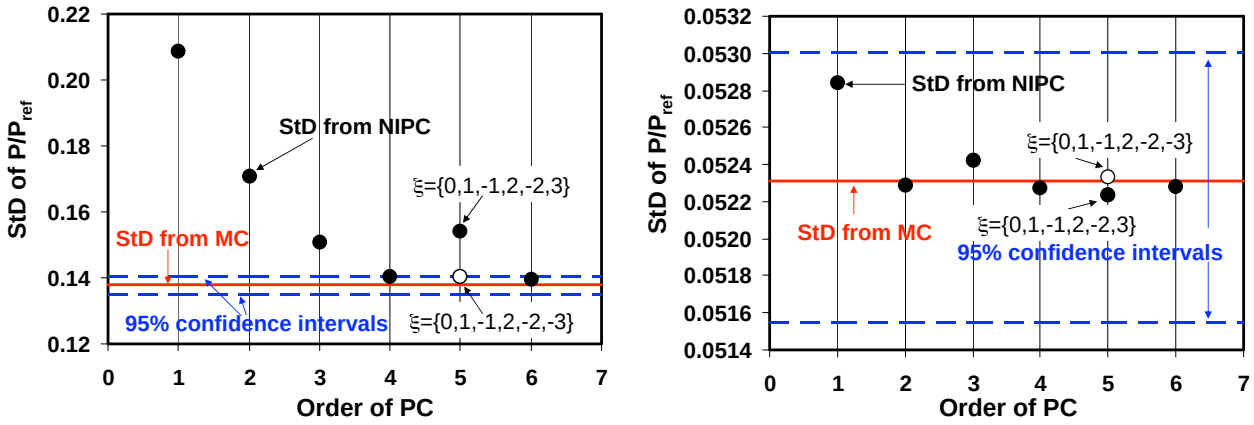

(a) Location 1 (Shock region)

(b) Location 2 (Downstream of shock)

Figure 7. The change in P/P_{ref} standard deviation values with the order of the polynomial expansions at locations 1 and 2. The deterministic Euler solutions are calculated using 3^{rd} order accurate upwind-biased Roe flux difference splitting with the MinMod limiter.

The histogram obtained with the 4^{th} order polynomial chaos method falls short in approximating the limit of the tail region which extends further right for the Monte Carlo distribution. The mean and the standard deviation of the polynomial chaos distribution fails to fall within the 95% confidence interval (Tables 2 and 3). Other two stations downstream of the shock again follow closely the normal distribution and the agreement between the Monte Carlo and polynomial chaos results is good. At locations 2 and 3, both mean and standard deviation values obtained with the NIPC method fall within the 95% confidence intervals.

To see the effect of the order of the polynomial chaos on the statistics, we have performed the NIPC analysis with different orders ranging from one to six. The deterministic Euler solutions with 3^{rd} order spatial accuracy were used to calculate the polynomial coefficients. Figure 6 shows the contours of pressure standard deviation difference between the results of Monte Carlo simulations and the NIPC method. For the 1^{st} order PC, the standard deviation values in the shock region are significantly different than those obtained with Monte Carlo simulations. Downstream of the shock, the difference is very small implying that the probability distributions of pressure in this region are Gaussian. A sixth order expansion seems to approximate the standard deviation well in the whole flow field, which proves that the pressure distributions across the shock region require sufficiently high order expansions to model the non-Gaussian contributions. One interesting observation from this figure is on the selection of the random vector. Despite the increase in order, if the additional random point is chosen from the positive side of the mean pressure (positive ξ values), the accuracy in the approximation of the standard deviation does not seem to improve as much as the case where the additional sampling point is chosen from the negative side of the mean. This observation suggests the importance of picking the optimum random vector for the efficiency of modeling the non-Gaussian output distributions with the current NIPC method.

To quantify the convergence of the standard deviation obtained with the NIPC method, we analyze the results at locations 1 (shock region) and 2 (downstream of the shock). Figure 7 shows the standard deviation of pressure obtained with different orders of polynomial expansions. For each location, Monte Carlo estimation of the standard deviation and the associated confidence interval is also presented. At location 2, standard deviation values obtained with all orders fall within the 95% confidence interval. Since the pressure distribution at this location is Gaussian (Figure 5), a first order expansion is sufficient to approximate the statistics. For location 1 which has a highly non-Gaussian and one-sided distribution due to the shock, only the standard deviation obtained with a sixth order polynomial expansion falls within the 95% confidence interval. With the increase of the order, standard deviation values converge monotonically to the Monte Carlo result except the fifth order case, which is obtained with solutions evaluated at random points, $\xi = \{0, 1, -1, 2, -2, 3\}$. A much better approximation is achieved by replacing the deterministic solution evaluated at $\xi = 3$ with the one obtained at $\xi = -3$, which corresponds to a wedge angle of $\theta = 3.5^o$. This observation re-emphasizes the importance of selecting the optimum random points for the evaluation of the coefficients of high order polynomial expansions when modeling non-Gaussian distributions.

The following equations give the sixth order polynomial chaos expansions of pressure scaled with the zeroth mode, a_0 (mean) at locations 1 and 2:

$$\left(\frac{P/P_{ref}(\xi)}{a_0}\right)_1 = 1.0 + 0.124017\xi + 0.0896966\xi^2 - 0.00174726\xi^3 - 0.0148230\xi^4 - 0.000100914\xi^5 + 0.000878693\xi^6$$

$$\left(\frac{P/P_{ref}(\xi)}{a_0}\right)_2 = 1.0 + 0.0362645\xi + 0.000503941\xi^2 - 0.0000884384\xi^3 - 0.0000204613\xi^4 + 7.11273 \times 10^{-6}\xi^5 + 2.08695 \times 10^{-6}\xi^6$$

At location 2, the contribution of second order or higher terms to the pressure distribution is small compared to the first two modes. For location 1, higher order terms of the expansion are significant due to the non-Gaussian nature of the pressure distribution.

B. Supersonic Expansion Wave Problem

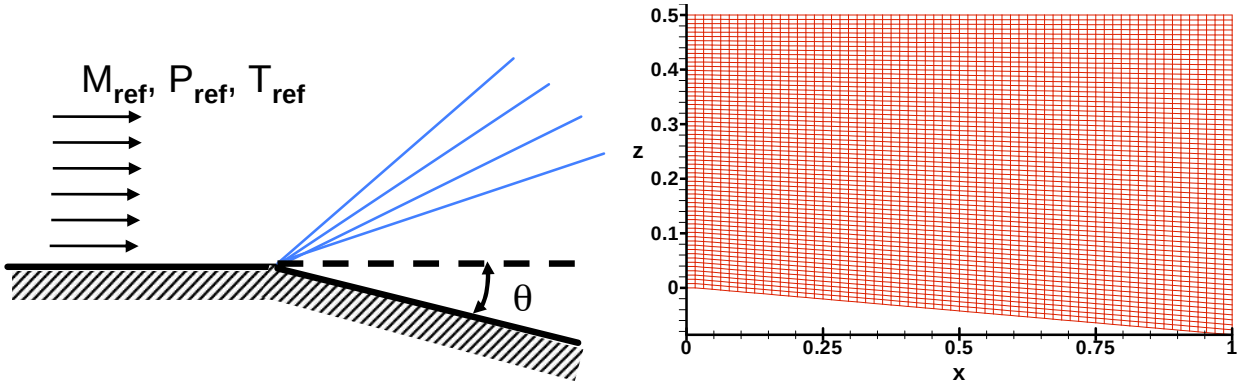

(a) Sketch of supersonic flow and the expansion wave.

(b) The mean grid (65×65) used in Euler computations. The mean deflection angle (θ_{mean}) is 5.0^o.

Figure 8. Description of the supersonic, inviscid flow over a convex corner with a turn angle of θ.

To analyze the stochastic expansion wave problem, we consider inviscid, steady, two-dimensional, supersonic flow of a calorically perfect gas over a convex corner. Under these conditions, a centered expansion fan originates from the sharp convex corner as shown in Figure 8(a). The static pressure, which is the output quantity of interest also for this problem, decreases continuously across the expansion fan and remains constant in the region downstream of the rearward Mach line. The deterministic problem involves the solution of the supersonic flow field for a given free stream Mach number (M_{ref}), specific heat ratio (γ), and the deflection angle (θ).

1. *Deterministic Problem*

To solve the deterministic problem, one may use the Prandtl-Meyer relations to calculate the Mach number at any increment of deflection angle across the expansion fan. Once the Mach number is known, the pressure drop (P/P_{ref}) can be calculated using the isentropic relations for a perfect gas. The details of the Prandtl-Meyer solution can be found in Anderson.[23] As in the oblique shock wave problem, we solved the deterministic problem numerically with the CFL3D code. Both NIPC and Monte Carlo methods used the deterministic solutions from Euler calculations in their implementation. The computations were performed on grids which have 65 grid points in both x- and z-directions. Figure 8(b) shows the grid with the mean deflection angle. The same boundary conditions, time integration scheme, and multigrid methods described for the oblique shock wave case were used in this problem to find the steady-state solutions. The free-steam Mach number was chosen as $M_{ref} = 3.0$ and the angle of attack was set to zero degrees. The inviscid fluxes on the cell-faces were again calculated using Roe flux difference splitting and the primitive variables on the cell faces were obtained using (1) a fully upwind 1^{st} order accurate interpolation, and (2) an upwind-biased 3^{rd} order accurate scheme with the $MinMod$ limiter.

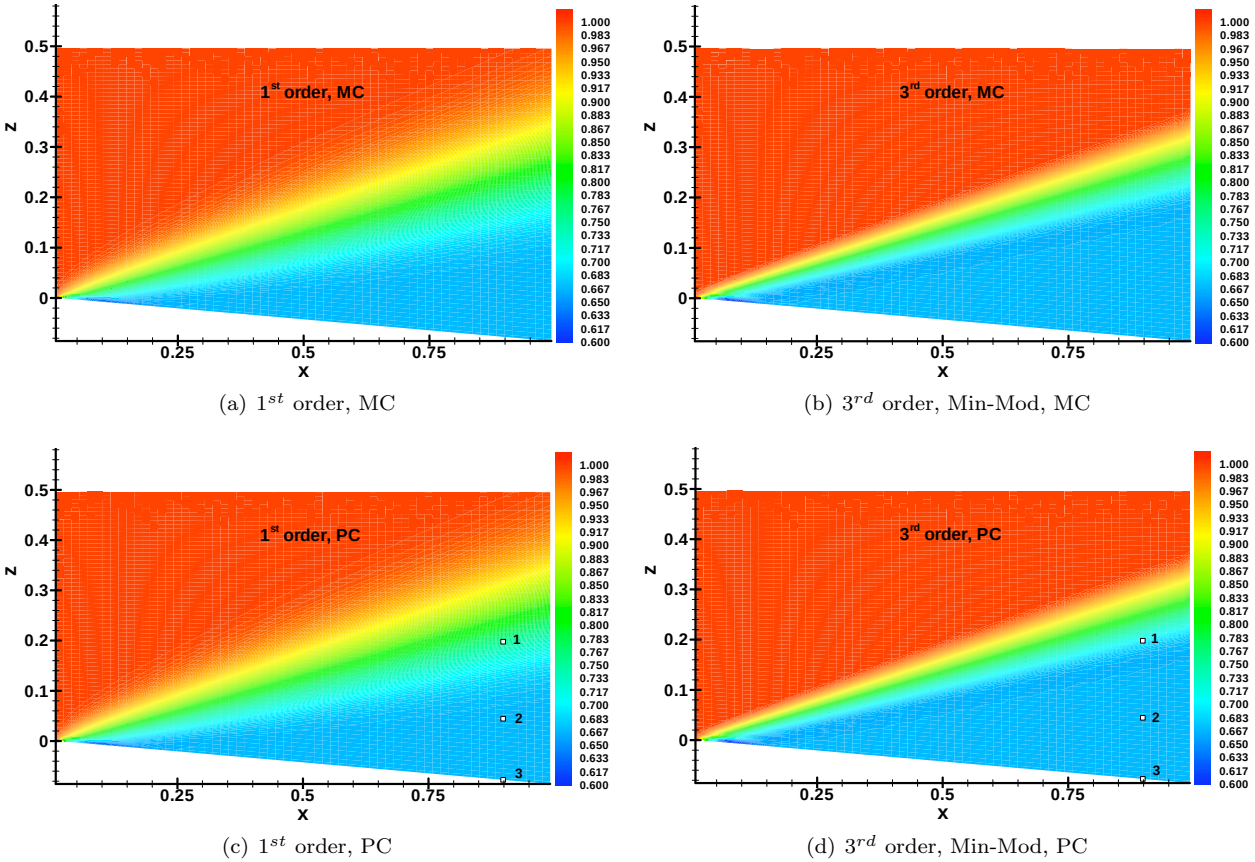

(a) 1^{st} order, MC

(b) 3^{rd} order, Min-Mod, MC

(c) 1^{st} order, PC

(d) 3^{rd} order, Min-Mod, PC

Figure 9. Mean pressure (P/P_{ref}) distributions obtained from MC simulations and NIPC method for the supersonic expansion problem. Polynomial chaos results are obtained with a 4^{th} order expansion. The three locations showed in the polynomial chaos plots designate the points where the quantitative analysis were performed.

Table 4. The mean static pressure (P/P_{ref}) values obtained with NIPC and Monte Carlo methods at three selected locations for the expansion wave problem. The 95% confidence intervals for the mean values are calculated for Monte Carlo simulations using the Bootstrap method.

Spatial Accuracy	Location	Mean PC	Mean MC	95% Conf. Interval
1^{st} *order*	1	0.756032	0.756048	[0.755834, 0.756276]
	2	0.668288	0.66829	[0.667744, 0.668849]
	3	0.668108	0.668108	[0.667558, 0.66867]
3^{rd} *order with MinMod*	1	0.697085	0.697122	[0.696907, 0.697336]
	2	0.668056	0.668065	[0.667515, 0.668629]
	3	0.668071	0.66807	[0.667519, 0.668633]

2. Stochastic Problem

Similar to the oblique shock wave example, the expansion wave problem was formulated by introducing a geometric uncertainty through the deflection angle ($\theta(\xi)$) that was described by a Gaussian distribution with a coefficient of variation of 10%. The mean deflection angle was chosen as $\theta_{mean} = 5^o$. Uncertainty propagation in supersonic expansion flow has been modeled using Monte Carlo and the non-intrusive polynomial chaos methods. In Monte Carlo simulations, 10,000 grids were created using 10,000 samples from the $\theta(\xi)$ distribution. The Euler Equations were solved on each grid using the CFL3D code. The uncertainty

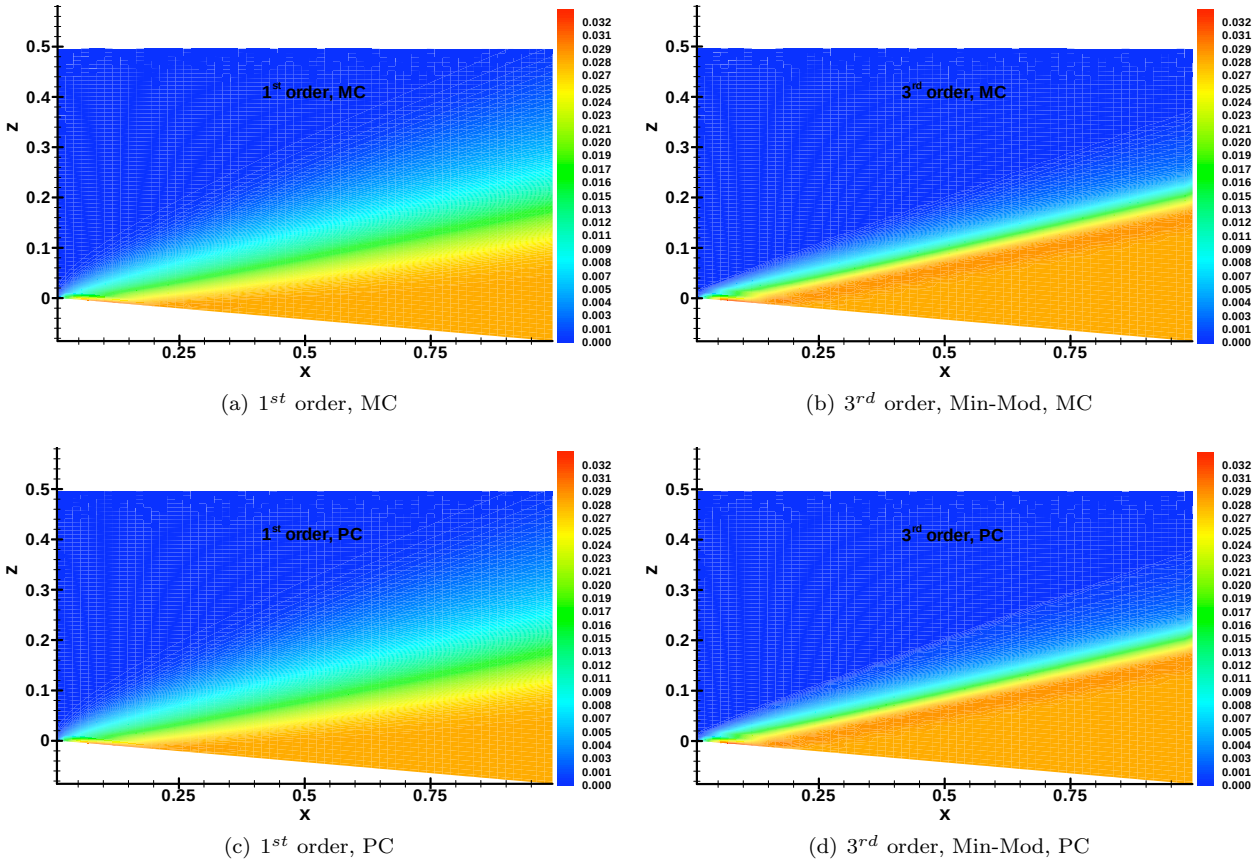

(a) 1^{st} order, MC

(b) 3^{rd} order, Min-Mod, MC

(c) 1^{st} order, PC

(d) 3^{rd} order, Min-Mod, PC

Figure 10. Standard deviation distributions of pressure (P/P_{ref}) obtained from MC simulations and NIPC method for the supersonic expansion problem. Polynomial chaos results are obtained with a 4^{th} order expansion.

Table 5. The standard deviation of static pressure (P/P_{ref}) obtained with NIPC and Monte Carlo methods at three selected locations for the expansion wave problem. The 95% confidence intervals for the standard deviations are calculated for Monte Carlo simulations using the Bootstrap method.

Spatial Accuracy	Location	StD PC	StD MC	95% Conf. Interval
1^{st} *order*	1	0.0114565	0.0114636	[0.01128, 0.0116386]
	2	0.027846	0.0278475	[0.0274421, 0.028226]
	3	0.0280006	0.0280007	[0.0275924, 0.0283773]
3^{rd} *order with MinMod*	1	0.0107491	0.010747	[0.010482, 0.0110103]
	2	0.0280358	0.0280317	[0.0276231, 0.0284082]
	3	0.0280277	0.028026	[0.0276174, 0.0284027]

propagation with the non-intrusive polynomial chaos method was modeled with a fourth order polynomial chaos expansion. To obtain the polynomial coefficients, five deterministic solutions were evaluated on five grids with deflection angles that correspond to $\xi_1 = 0.0$, $\xi_2 = 1.0$, $\xi_3 = -1.0$, $\xi_4 = 2.0$, and $\xi_5 = -2.0$.

Figure 9 gives the mean pressure contours of the NIPC method and the Monte Carlo simulations. For the same spatial accuracy, the qualitative agreement between the results of the two methods is good. Across the expansion wave, all cases show a smooth mean pressure drop, however the expansion wave is wider for the cases with 1^{st} order spatial accuracy. The contours of standard deviation again show a good qualitative agreement between the Monte Carlo and the polynomial chaos results (Figure 10). The standard deviation

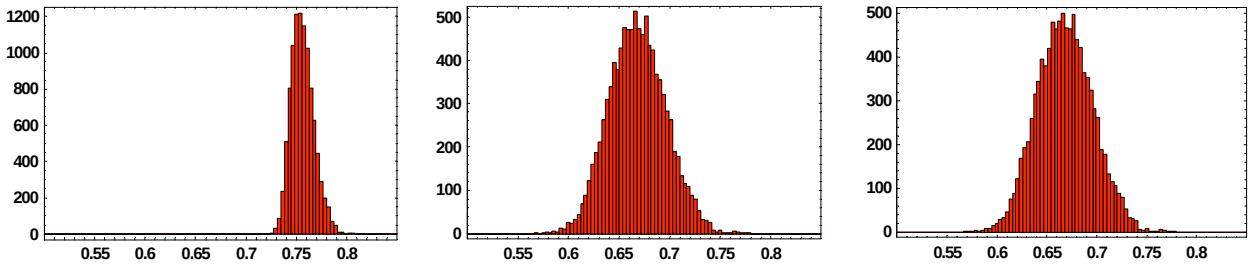

(a) Location 1, MC (b) Location 2, MC (c) Location 3, MC

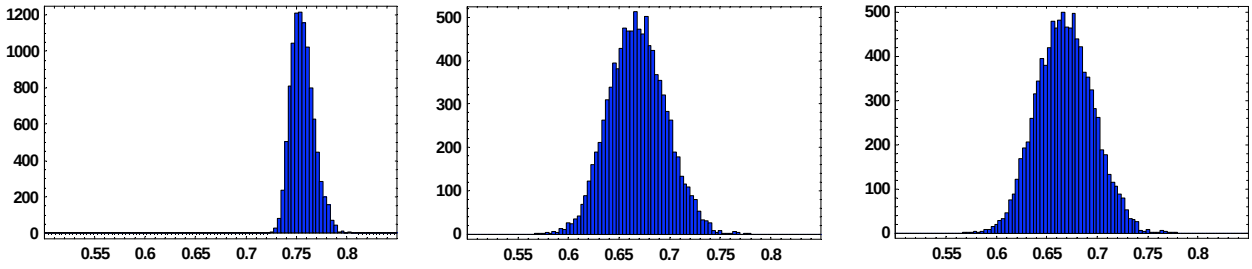

(d) Location 1, PC (e) Location 2, PC (f) Location 3, PC

Figure 11. Static pressure histograms obtained at three locations for the supersonic expansion wave problem using MC and NIPC methods. The deterministic Euler solutions are calculated using 1^{st} order accurate upwind-biased Roe flux difference splitting. Polynomial chaos results are obtained from a 4^{th} order expansion.

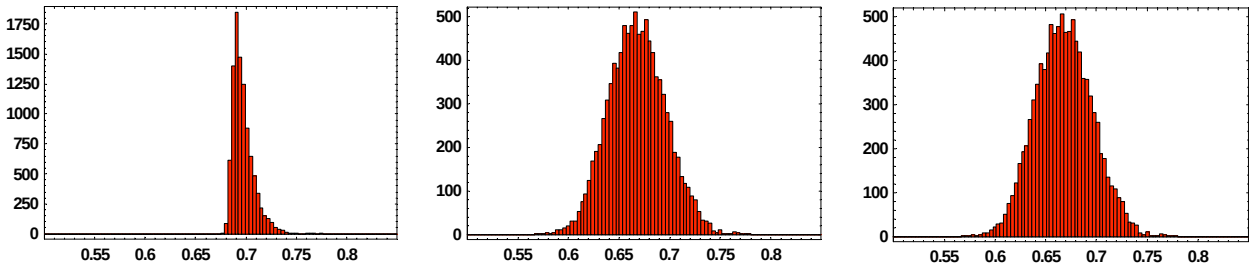

(a) Location 1, MC (b) Location 2, MC (c) Location 3, MC

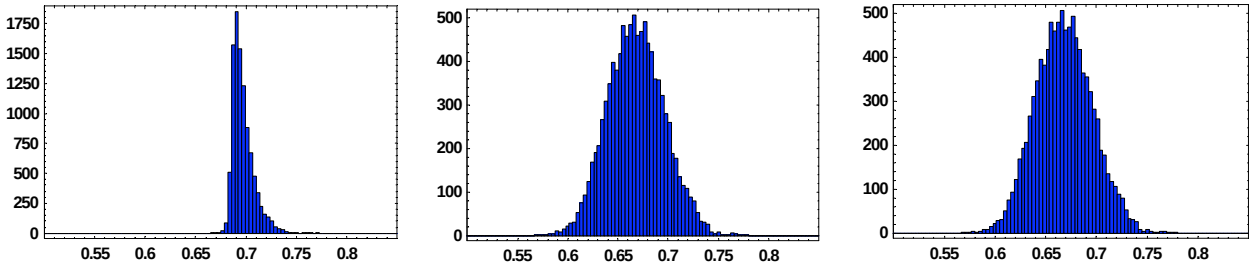

(d) Location 1, PC (e) Location 2, PC (f) Location 3, PC

Figure 12. Static pressure histograms obtained at three locations for the supersonic expansion wave problem using MC and NIPC methods. The deterministic Euler solutions are calculated using 3^{rd} order accurate upwind-biased Roe flux difference splitting with MinMod limiter. Polynomial chaos results are obtained from a 4^{th} order expansion.

increases smoothly across the expansion wave for all cases. This change occurs again in a wider region for the 1^{st} order spatially accurate solutions.

As in the oblique shock wave problem, we picked three locations in the flow field to compare the statistics of the Monte Carlo and NIPC methods quantitatively. Again these points are on the same streamwise station, but they are at different distances from the wall (Figure 9). Location 1 ($x = 0.8984$, $z = 0.1978$) is

in the expansion fan towards the rearward Mach line, Location 2 ($x = 0.8984$, $z = 0.0445$) is downstream of the expansion fan, and Location 3 ($x = 0.8984$, $z = -0.0772$) is a point on the wall downstream of the expansion fan. The static pressure histograms at these locations are shown in Figure 11 for the 1^{st} order spatially accurate deterministic Euler solutions. At all locations, the histograms of the non-intrusive polynomial chaos method are in good agreement with the ones obtained with the Monte Carlo simulations. The distribution at location 1 (expansion fan) is slightly skewed to the right, whereas the histograms at locations 2 and 3 follow the Gaussian distribution closely. For all three locations, the mean and standard deviation values obtained with the NIPC method fall within the 95% confidence intervals that were calculated for the statistics of Monte Carlo simulations using the *bootstrap method* (Tables 4 and 5). For the 3^{rd} order spatially accurate solutions, the pressure distribution at location 1 is non-Gaussian and skewed to the right with a significant tail (Figure 12). The NIPC can accurately approximate the shape of the histogram at this location and both statistics fall within the corresponding 95% confidence intervals. These results indicate that a 4^{th} order polynomial expansion is sufficient to model the non-Gaussian contributions observed at this region of the flow. The pressure histograms at the other stations again follow a normal distribution and the results of the Monte Carlo and the non-intrusive polynomial chaos methods are in very good agreement. Table 5 shows that the standard deviation at location 1 is approximately 2.5 times less than the ones obtained at locations 2 and 3 for both orders of spatial accuracy. These results can also be detected visually from the histogram plots.

C. Laminar Boundary Layer Flow over a Flat Plate

To analyze the stochastic laminar boundary layer problem, we consider a steady, subsonic, two-dimensional, zero-pressure gradient flow over a flat plate (Figure 13). The Reynolds number obtained with the mean value of the dynamic viscosity is $Re_{mean} = 2 \times 10^5$ at $x = 0.7375$, which indicates that the boundary layer is laminar. Mach number of the free-stream flow is $M_\infty = 0.3$. The velocity profile (u/U_∞), boundary layer thickness (δ), displacement thickness (δ^*), and the momentum thickness (θ) at $x = 0.7375$ are the quantities of interest for this problem.

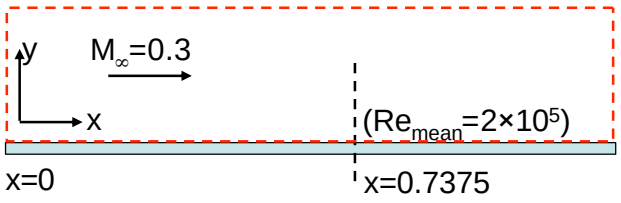

Figure 13. Description of the stochastic laminar boundary layer problem which has an input uncertainty in the dynamic viscosity of the free-stream.

1. *Deterministic Problem*

The deterministic solution to an incompressible laminar boundary layer flow with zero pressure gradient can be obtained with the Blasius solution. The details of this approach can be found in White.[24] In our study, we used the Blasius solution both for NIPC method and Monte Carlo simulations.

2. *Stochastic Problem*

The stochastic laminar boundary layer flow problem is formulated by modeling the dynamic viscosity of the free-stream (μ_∞) as a normally distributed stochastic parameter with a coefficient of variation of 2%. The rest of the free-stream flow properties (the density, velocity, and the pressure) were treated as deterministic parameters and kept constant for all the simulations. The histogram of the free-stream dynamic viscosity is shown in Figure 14, which was created with 10,000 random samples from the nor-

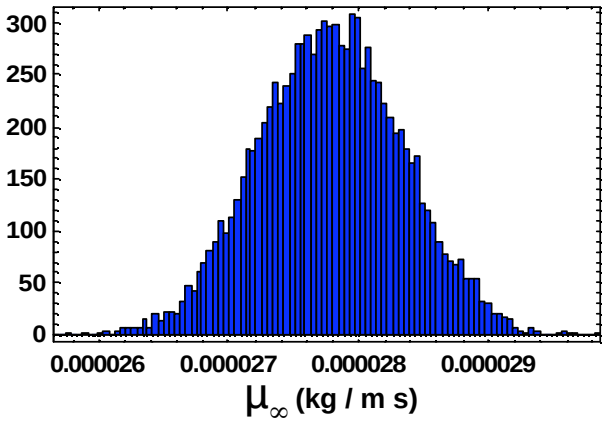

Figure 14. Histogram showing the uncertainty in the free-stream dynamic viscosity which is modelled as a normally distributed stochastic parameter with a coefficient of variation (CoV) of 2%.

mal population represented by

$$\mu_\infty(\xi) = \overline{\mu_\infty} + \xi\sigma. \tag{14}$$

Here $\overline{\mu_\infty}$ is the mean value of the free-stream dynamic viscosity, σ is the standard deviation, and ξ is again a normally distributed random variable with zero mean and unit variance.

The uncertainty propagation in the laminar boundary layer problem was modeled with two different methods: Monte Carlo and the NIPC. A total number of 10,000 Monte Carlo simulations were performed to get the statistics of the uncertainty in different output quantities. Each realization was obtained by applying the Blasius solution to the problem for each dynamic viscosity sample. A fourth order polynomial chaos expansion was chosen to model the stochastic variables in the NIPC method. To calculate the polynomial coefficients, five deterministic Blasius solutions were obtained for five dynamic viscosity values which correspond to the random variables at $\xi_1 = 0.0$, $\xi_2 = 1.0$, $\xi_3 = -1.0$, $\xi_4 = 2.0$, and $\xi_5 = -2.0$.

The statistics (mean and standard deviation) of different output variables obtained from the NIPC method and Monte Carlo simulations are compared at $x = 0.7375$. Figure 15 shows the standard deviation of u/U_∞ through the boundary layer at this station. Here, u is the velocity component in x-direction and U_∞ is the free-stream velocity. The standard deviation profile of u/U_∞ and the histograms of the boundary layer quantities (Figure 16) at x=0.7375 show nearly perfect agreement between Monte Carlo and non-intrusive PC results. The numerical comparison of the boundary layer statistics are given in Table 6. Both mean and standard deviation of all boundary layer quantities are the same up to five significant digits. All boundary layer quantities exhibit a normal distribution with a coefficient of variation of approximately 1%. It should be noted that polynomial chaos expansions required five deterministic calculations and the solution of one linear problem for five unknown coefficients, whereas Monte Carlo Simulations required 10,000 deterministic runs.

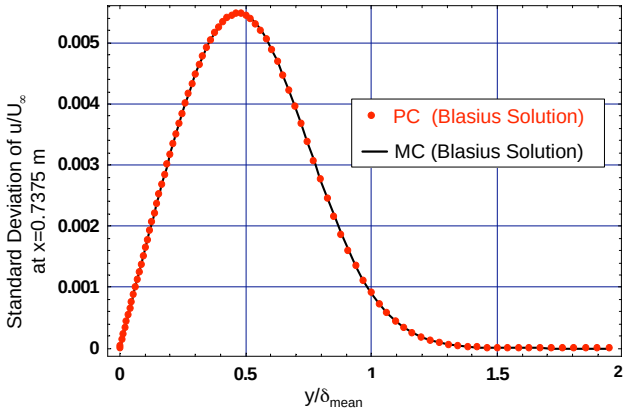

Figure 15. Standard deviation of u/U_∞ at $x = 0.7375$ m.

The coefficients of polynomial chaos expansions obtained for each boundary layer quantity at $x = 0.7375$ are given in Table 7. The coefficients of the 2^{nd} order terms (a_2) are approximately three orders of magnitude less than those obtained for the 1^{st} order terms (a_1). For the higher order terms, the coefficients decrease

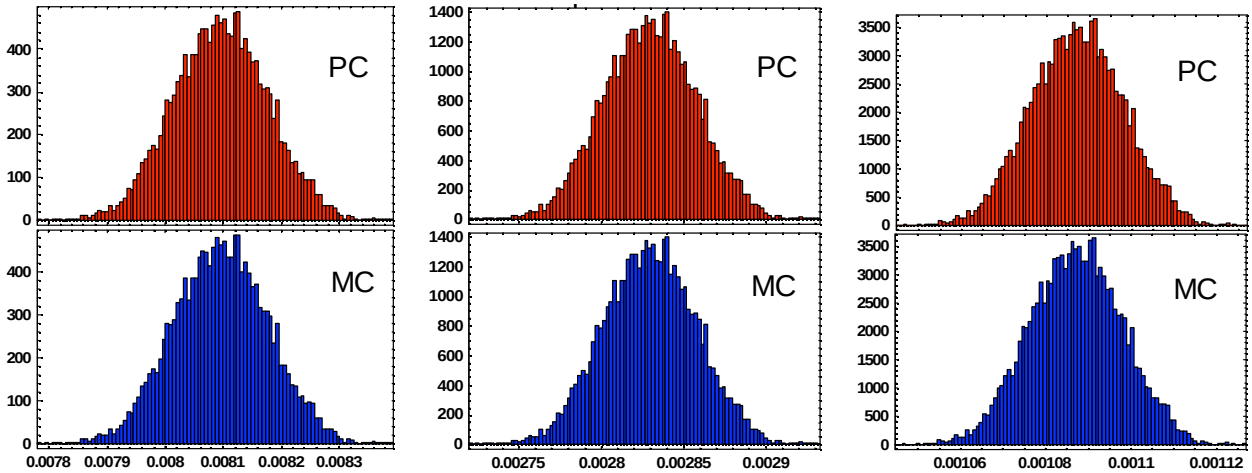

(a) δ (m) (b) $\delta*$ (m) (c) θ (m)

Figure 16. Histograms of the boundary layer quantities at $x = 0.7375$ obtained with the NIPC method (Blasius solution) and with the Monte Carlo simulations (Blasius solution).

Table 6. Statistics of the boundary layer quantities at $x = 0.7375$.

	Boundary Layer Thickness		Displacement Thickness		Momentum Thickness	
Statistics	**PC**	**MC**	**PC**	**MC**	**PC**	**MC**
Mean $\times 10^3$ ***(m)***	8.09683	8.09681	2.82954	2.82954	1.08712	1.08712
STD $\times 10^5$ ***(m)***	8.08945	8.08933	2.82695	2.82696	1.08612	1.08612
CoV $\times 10^2$	0.99909	0.99908	0.99908	0.99909	0.99908	0.99908

Table 7. The coefficients of polynomial chaos expansions ($\cdots = a_0 + a_1\xi + a_2\xi^2 + a_3\xi^3 + a_4\xi^4$) obtained for each boundary layer quantity at $x = 0.7375$.

Boundary Layer Quantity	$\delta(\xi)$ (m) $(\delta(\xi)/a_0)$	$\delta^*(\xi)$ (m) $(\delta^*(\xi)/a_0)$	$\theta(\xi)$ (m) $(\theta(\xi)/a_0)$
a_0	8.09731×10^{-3}	2.82971×10^{-3}	1.08718×10^{-3}
(a_0/a_0)	(1.0)	(1.0)	(1.0)
a_1	8.09731×10^{-5}	2.82969×10^{-5}	1.08717×10^{-5}
(a_1/a_0)	(10^{-2})	(9.99993×10^{-3})	(9.99991×10^{-3})
a_2	-4.04865×10^{-7}	-1.41295×10^{-7}	-5.47285×10^{-8}
(a_2/a_0)	$(-4.99999 \times 10^{-5})$	$(-4.99327 \times 10^{-5})$	$(-5.033987 \times 10^{-5})$
a_3	4.05220×10^{-9}	1.44526×10^{-9}	5.80316×10^{-10}
(a_3/a_0)	(5.00438×10^{-7})	(5.10745×10^{-7})	(5.33781×10^{-7})
a_4	5.06614×10^{-11}	-5.40440×10^{-11}	7.12134×10^{-11}
(a_4/a_0)	(6.25657×10^{-9})	$(-1.90988 \times 10^{-8})$	(6.55028×10^{-8})

by approximately two orders of magnitude per degree. This is an expected result, since all boundary layer quantities at this station exhibit a Gaussian distribution (Figure 16).

The results of this test case indicate that non-intrusive polynomial chaos method can accurately model the propagation of an input uncertainty and accurately predict the statistics of an output variable for this laminar boundary layer flow problem.

V. Conclusions

An inexpensive NIPC method for the propagation of input uncertainty in CFD simulations has been presented. The method described here is non-intrusive in the sense that no modification to the deterministic code is required. The present method is straightforward to implement for any stochastic fluid dynamics problem and computationally less expensive than sampling or quadrature based non-intrusive methods.

To test the performance of this NIPC approach, the method has been applied to three stochastic fluid dynamics problems: (1) inviscid oblique shock wave problem with geometric uncertainty, (2) inviscid supersonic expansion wave problem with geometric uncertainty, and (3) steady, subsonic, 2-D, zero-pressure gradient laminar boundary layer flow over a flat plate, which has the free-stream dynamic viscosity as the uncertain parameter. For each test case, the polynomial chaos results were compared to the statistics obtained with the Monte Carlo simulations.

The results of the stochastic test cases showed the efficiency and the accuracy of the present NIPC method in uncertainty propagation. For all three stochastic test problems, the statistics (mean and the standard deviation) obtained with the NIPC method were in good agreement with the results of the Monte Carlo simulations. In the oblique shock wave case, the shape of static pressure distributions obtained with

3^{rd} order spatially accurate Euler solutions were highly non-Gaussian in the shock region, and a sixth order polynomial expansion was required to estimate the statistic within the 95% confidence intervals of the Monte Carlo results. For other regions, a fourth order polynomial chaos expansion was sufficient to obtain the statistics with the desired accuracy. The stochastic study on the shock region also suggested the importance of selecting the optimum random vector for the efficiency of modeling the non-Gaussian output distributions with the current NIPC method. In the expansion wave and the boundary layer problem, the polynomial chaos statistics obtained with a fourth order expansion were in good agreement with the Monte Carlo results.

The future work will include the investigation of adaptive sampling techniques for efficient calculation of polynomial chaos coefficients that are important to the response of interest. Future plans also include the application of the current method to large scale aerospace problems and the exploration of robust and risk based design using non-intrusive polynomial chaos methods.

References

[1]Hosder, S., Grossman, B., Watson, L. T., Mason, W. H., and Haftka, R. T., "Observations on CFD Simulation Uncertainties, AIAA Paper 2002-5531," 9^{th} *AIAA/ISSMO Symposium on Multidisciplinary Analysis and Optimization*, Atlanta, GA, September, 2002.

[2]Hemsch, M. J., "Statistical Analysis of CFD Solutions from the Drag Prediction Workshop, AIAA Paper 2002-0842," 40^{th} *AIAA Aerospace Sciences Meeting and Exhibit*, Reno, NV, January, 2002.

[3]Walters, R. W. and Huyse, L., "Uncertainty Analysis for Fluid Mechanics with Applications," Tech. rep., ICASE 2002-1, NASA/CR-2002-211449, NASA Langley Research Center, Hampton, VA, 2002.

[4]Ghanem, R. and Spanos, P. D., "Polynomial Chaos in Stochastic Finite Elements," *Journal of Applied Mechanics*, Vol. 57, March 1990, pp. 197–202.

[5]Ghanem, R., "Stochastic Finite Elements with Multiple Random Non-Gaussian Properties," *Journal of Engineering Mechanics*, January 1999, pp. 26–40.

[6]Ghanem, R. G., "Ingredients for a General Purpose Stochastic Finite Element Formulation," *Computational Methods in Applied Mechanical Engineering*, Vol. 168, 1999, pp. 19–34.

[7]L. Mathelin, M.Y. Hussaini, T. Z. and Bataille, F., "Uncertainty Propagation for Turbulent, Compressible Nozzle Flow Using Stochastic Methods," *AIAA Journal*, Vol. 42, No. 8, August 2004, pp. 1669–1676.

[8]Xiu, D. and Karniadakis, G. E., "Modeling Uncertainty in Flow Simulations via Generalized Polynomial Chaos," *Journal of Computational Physics*, Vol. 187, No. 1, May 2003, pp. 137–167.

[9]Wiener, N., "The Homogeneous Chaos," *American Journal of Mathematics*, Vol. 60, No. 4, 1938, pp. 897–936.

[10]Walters, R., "Towards stochastic fluid mechanics via Polynomial Choas-invited, AIAA-Paper 2003-0413," 41^{st} *AIAA Aerospace Sciences Meeting and Exhibit*, Reno, NV, January, 2003, CD-ROM.

[11]Perez, R. and Walters, R., "An Implicit Compact Polynomial Chaos Formulation for the Euler Equations, AIAA-Paper 2005-1406," 43^{rd} *AIAA Aerospace Sciences Meeting and Exhibit*, Reno, NV, January, 2005, CD-ROM.

[12]Debusschere, B. J., Najm, H. N., Pebay, P. P., Knio, O. M., Ghanem, R. G., and Maitre, O. P. L., "Numerical Challenges in the Use of Polynomial Chaos Representations for Stochastic Processes," *SIAM Journal on Scientific Computing*, Vol. 26, No. 2, 2004, pp. 698–719.

[13]Reagan, M., Najm, H. N., Ghanem, R. G., and Knio, O. M., "Uncertainty Quantification in Reacting Flow Simulations through Non-Intrusive Spectral Projection," *Combustion and Flame*, Vol. 132, 2003, pp. 545–555.

[14]Isukapalli, S. S., "Uncertainty Analysis of Transport-Transformation Models, PhD Dissertation," Tech. rep., Rutgers, The State University of New Jersey, New Braunswick, NJ, 1999.

[15]L. Mathelin, M.Y. Hussaini, T. Z., "Stochastic Approaches to Uncertainty Quantification in CFD Simulations," *Numerical Algorithms*, Vol. 38, No. 1, March 2005, pp. 209–236.

[16]Ghanem, R. G. and Spanos, P. D., *Stochastic Finite Elements: A Spectral Approach*, Springer-Verlag, New York, 1991.

[17]Xiu, D. and Karniadakis, G. E., "The $Wiener - Askey$ Polynomial Chaos for Stochastic Differential Equations," Tech. Rep. 01-1, Center for Fluid Mechanics, Division of Applied Mathematics, Brown University, Providence, RI, 2001.

[18]Wiener, N. and Wintner, A., "The Discrete Chaos," *American Journal of Mathematics*, Vol. 65, No. 2, 1943, pp. 279–298.

[19]Walters, R., "Optimization and Reconstruction via the Polynomial Chaos," *Proceedings of the Sixth European Conference on Structural Dynamics*, Paris, France, September, 2005, CD-ROM.

[20]Krist, S. L., Biedron, R. T., and Rumsey, C. L., "CFL3D User's Manual (Version 5.0)," Tech. rep., NASA TM-1998-208444, NASA Langley Research Center, Hampton, VA, 1998.

[21]Roe, P. L., "Approximate Riemann Solvers, Parameter Vectors, and Difference Schemes," *Journal of Computational Physics*, Vol. 43, 1981.

[22]Roy, C. J., "Grid Convergence Error Analysis for Mixed-Order Numerical Schemes, AIAA Paper 2001-2606," *AIAA* 15^{th} *Computational Fluid Dynamics Conference*, Anaheim, CA, June 2001.

[23]Anderson, J. D., *Modern Compressible Flow with Historical Perspective, Third Edition*, McGraw-Hill, New York, USA, 2003.

[24]White, F. M., *Viscous Fluid Flow*, McGraw-Hill, Inc., 1974.